Acetylene Derivatives of Cationic Diazaoxatriangulenes and Diaza [4]Helicenes - Access to Red Emitters and Planar Chiral Stereochemical Traits

Pavol Ondrisek,[a] Margaux Elie,[a] Marion Pupier,[a] Adiran de Aguirre,[a] Amalia I. Poblador-Bahamonde,[a] Céline Besnard,[b] and Jérôme Lacour*[a]

Abstract: Cationic triangulenes, and related helicenes, constitute a rich class of dyes and fluorophores, usually absorbing and emitting light at low energy, in the orange to red domains. Recently, to broaden the scope of applications, regioselective late-stage functionalizations on these core moieties have been developed. For instance, with the introduction of electron-donating groups (EDGs), important bathochromic shifts are observed pushing absorptions towards or in the near-infrared (NIR) spectral domain while emissive properties disappear essentially completely. Herein, to upset this drawback, acetylene derivatives of cationic diazaoxa triangulenes (DAOTA) and [4]helicenes are prepared (16 examples). Contrary to other EDG-functionalized derivatives, C≡C− functionalized products remain broadly fluorescent, with red-shifted absorptions ($\Delta\lambda_{abs}$ up to 25 nm) and emissions ($\Delta\lambda_{em}$ up to 73 nm, Φ_{PL} up to 51%). Quite interestingly, a general dynamic stereoisomerism phenomenon is evidenced for the compounds derived from achiral DAOTA cores. At low temperature in ^{1}H NMR spectroscopy (218 K), N−CH$_2$ protons become diastereotopic with chemical shifts differences ($\Delta\delta$) as high as +1.64 ppm. The signal coalescence occurs around 273 K with a barrier of ∼12 kcal mol^{-1}. This phenomenon is due to planar chiral conformations (S_p and R_p configurations), induced by the geometry of the alkyl (n-propyl) side-chains next to the acetylenic substituents. Ion pairing studies with Δ-TRISPHAT anion not only confirm the occurrence of the chiral conformations but evidence a moderate but definite asymmetric induction from the chiral anion onto the cations. Finally, DFT calculations offer a valuable insight on the geometries, the corresponding stereodynamics and also on the very large difference in NMR for some of the diastereotopic protons.

Introduction

Chiral cationic [4]helicenes and their achiral diazaoxa triangulene counterparts, DMQA **1** and DAOTA **2** respectively (Figure 1), constitute a rich class of dyes and fluorophores that are related to triarylcarbenium ions.[1] In these structures, thanks to the presence of bridging electron-rich heteroatoms, improved charge delocalization and electronic stabilization occur and enhance the rich photophysics and redox chemistry of the
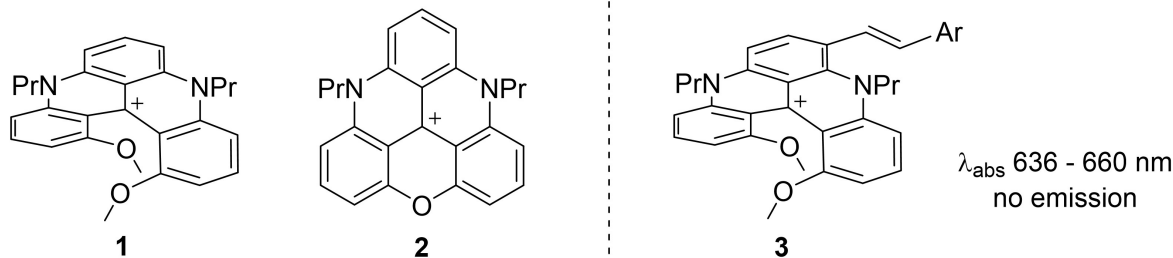
[a] P. Ondrisek, Dr. M. Elie, M. Pupier, Dr. A. de Aguirre, Dr. A. I. Poblador-Bahamonde, Prof. J. Lacour
Department of Organic Chemistry
University of Geneva
Quai Ernest Ansermet 30, 1211 Geneva 4 (Switzerland)
E-mail: jerome.lacour@unige.ch

[b] Dr. C. Besnard
Laboratoire de Cristallographie
University of Geneva
Quai Ernest Ansermet 24, 1211 Geneva 4 (Switzerland)

cationic π-systems.[2] Quite a few applications in domains as varied as analytics, biochemistry and biology,[3] catalysis and synthesis,[4] (chir)optical spectroscopy,[5] physics and surface sciences[6] have been reported for these two classes of compounds. Recently, to extend the range and scope of possible applications, regioselective late-stage functionalizations of compounds **1** and **2** have been achieved, giving the possibility to address discrete properties even further. Functionalized DMQA and DAOTA derivatives were prepared carrying either electron-withdrawing groups (EWGs) or electron-donating groups (EDGs), ∼25 and 10 examples respectively.[7] In both series, EWGs induce blue-shifted transitions in absorption and in emission. In addition, in fluorescence, quantum yields were found to increase in correlation with the strength of the electron-poor auxochrome substituent. With EDGs, important bathochromic shifts are observed pushing absorptions towards or in the near-infrared (NIR) spectral domain; emissive properties disappearing however essentially completely.[8] In fact and of importance for the current study, the substitution of DMQA derivatives with styryl moieties (**3**) is sufficient to provoke a red-shift of the absorption ($\Delta\lambda_{max} > 20$ nm) but also forego the fluorescence, even when the olefin side chains are substituted with phenyl groups carrying strong EWGs. Effective conjugation and donor-ability of double-bonds are hence sufficient to hamper the luminescence.

Chemistry–A European Journal

Research Article
doi.org/10.1002/chem.202104405

Chemistry Europe
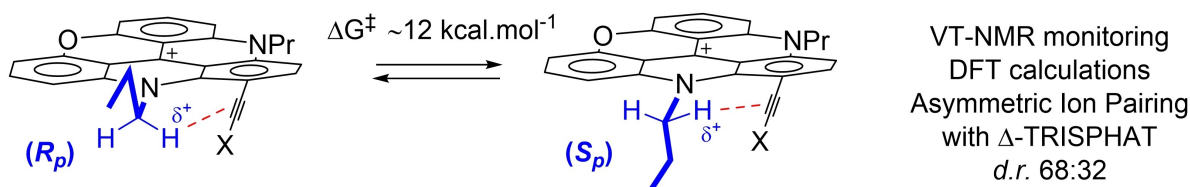European Chemical
Societies Publishing

Figure 1. Structures and optical properties of the previously reported DMQA and DAOTA derivatives and new studied compounds. Pr stands for n-Propyl side chains.

Herein, in a new development to fine-tune the optical properties of DMQA **1** and DAOTA **2**, acetylene derivatives **4** and **5** were prepared by late-stage functionalization of the main skeletons. Contrary to styryl derivatives **3**,[7a] these compounds remain fluorescent for the most part. These series are thus the best compromise to achieve both red-shifted absorptions ($\Delta\lambda_{abs}$ up to 25 nm) and emissions ($\Delta\lambda_{em}$ up to 73 nm, Φ_{PL} up to 51%). In addition, and importantly, a general dynamic stereoisomerism phenomenon can be evidenced for achiral compounds **5**, as demonstrated by ^{1}H NMR spectroscopic analyses and variable temperature (VT) studies in particular. At low temperature (263 K and below), certain methylene protons become diastereotopic with chemical shifts differences ($\Delta\delta$) as high as +1.64 ppm between the anisochronous hydrogens. The signal coalescence occurs around 273 K and a barrier of ~12 kcal mol^{-1}

is measured for the stereodynamic exchange. This phenomenon is due to planar chiral conformations (S_p and R_p configurations), induced by the geometry of the alkyl (n-propyl) side-chains next to the acetylenic substituents. Ion pairing studies with Δ-TRISPHAT anion not only confirmed the occurrence of the chiral conformations but evidenced a moderate but clearly defined asymmetric induction from the anion onto the cation. Finally, X-ray crystallographic analyses and DFT calculations have offered a valuable insight on the geometries, the corresponding stereodynamics and also on the very large difference in NMR for some of the diastereotopic protons.

Chemistry–A European Journal

Research Article
doi.org/10.1002/chem.202104405

Chemistry Europe
European Chemical
Societies Publishing

Results and Discussion

Formation of acetylene derivatives **4** and **5** was achieved following homologous synthetic routes (Scheme 1). In the DMQA series, substrate **1** was subjected to a Vilsmeier-Haack (VH) formylation to obtain [4]helicene aldehyde **6** in 82% yield; the reaction is readily scalable to a 5 g scale (10 mmol).[7a] Then, homologation to terminal alkyne **4a** was achieved under classical Ohira-Bestmann conditions (66% yield).[9] Finally, to form aryl-substituted **4b** to **4h**, cross-coupling reactions were performed under Cu/Pd-catalyzed Sonogashira conditions and afforded the desired products in moderate to good yields (69%–77%). In the DAOTA series, direct formylation of triangulene **2** was possible under VH conditions but complex crude mixtures were obtained containing minor amounts of regioisomeric aldehydes and products of poly-substitution. Purification of **7** by recrystallization was thus necessary causing large variations in yields from one batch to the next (20%–65%).[7b] To streamline the synthesis, a more robust route was developed by treatment of aldehyde **6** with boron tribromide to induce

the O-ring closure upon demethylation and formation of **7** in excellent and reproducible isolated yield (88%). Then, using the same elongation conditions as in the DMQA series, terminal alkyne **5a** (71%) and then aryl-substituted **5b** to **5h** were readily prepared (60%–88%). Full characterization of compounds **4** and **5** are presented in the Supporting Information file and included dataset. All data correspond to classical expectations to the exception of the room-temperature ^{1}H NMR spectra of compounds **5**. The observed phenomenon will be later discussed in the course of this article.

For both compounds **4** and **5**, structural information was readily gathered by single-crystal X-ray diffraction analysis. For compounds **4c**, **4d**, **4f** and **5c**, crystals suitable for measurements were obtained by layering (Table 1). Not surprisingly, the resulting structures present many similarities in term of bond lengths, including the triple bond 1.20 Å distance and the 1.42/1.43 Å connections to the aromatic frameworks (Table 1, entries 1 & 2). None of C≡C bonds present a strict linear arrangement; structures **4c**, **4d**, **4f** and **5c** displaying angles of 177.6°, 176.3° and 172.0° and 169.5° values respectively
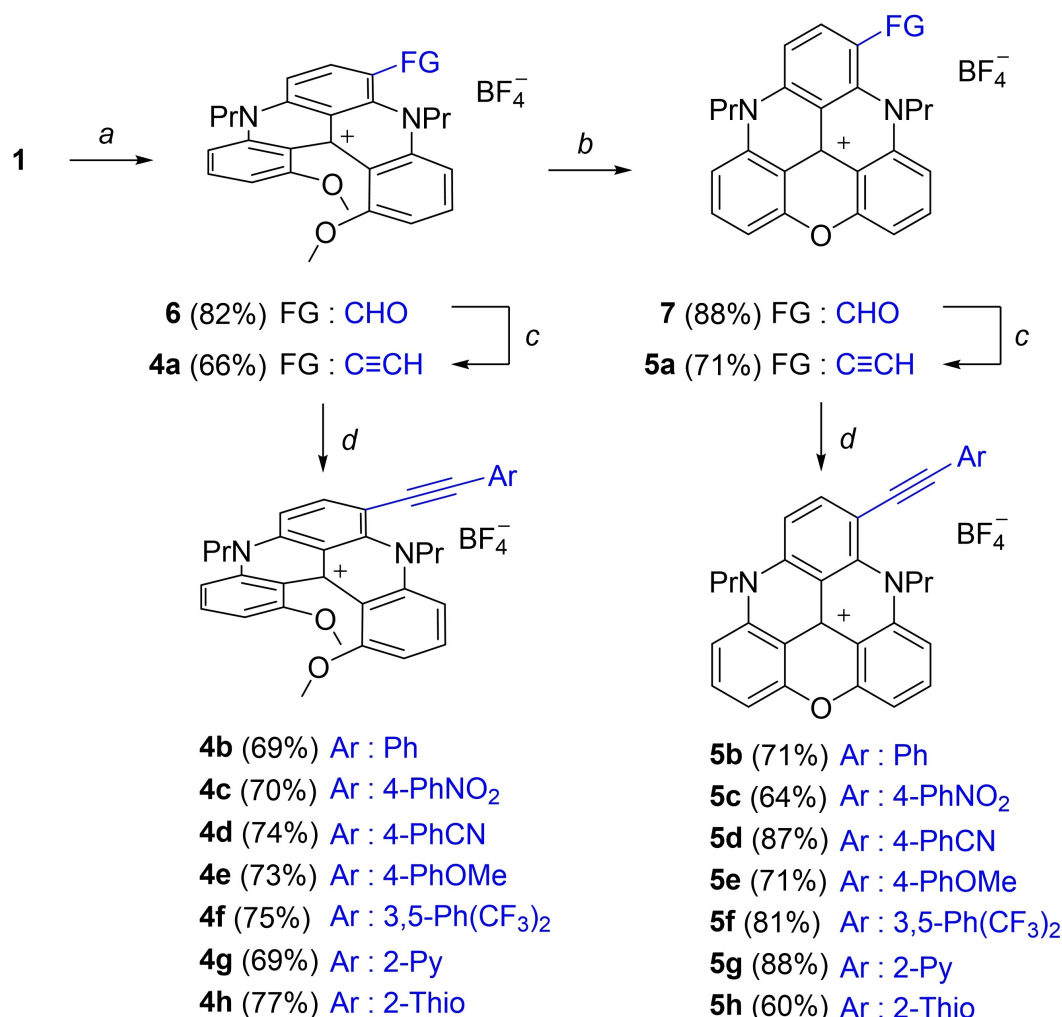
Scheme 1. Synthesis of products **4** and **5**. FG = functional group. a) DMF (24 equiv.), POCl₃ (48 equiv.), 90 °C, 3 h. b) BBr₃ (3×1.0 equiv.), 0–25 °C, CH₂Cl₂. c) Dimethyl (1-diazo-2-oxopropyl)phosphonate (2 equiv.), K₂CO₃ (3 equiv.), MeOH, 25 °C, 5–16 h. d) Pd₂dba₃ (2.5 mol%), PPh₃ (12.5 mol%), CuI (5 mol%), aryl iodide (3 equiv.), 1,2-dichloroethane/triethylamine (3:1), 75 °C, 3–5 h.

Chem. Eur. J. **2022**, *28*, e202104405 (3 of 11)

© 2022 The Authors. Chemistry - A European Journal published by Wiley-VCH GmbH

Chemistry–A European Journal

Research Article
doi.org/10.1002/chem.202104405

Chemistry Europe
European Chemical
Societies Publishing

Table 1. Crystal structures of **4c** (**A**), **4d** (**B**), **4f** (**C**) and **5c** (**D**). Hydrogen atoms and the counterions omitted for clarity. Selected bond lengths (Å), angles (°) and geometrical parameters.[a]


Entry		4c	4d	4f	5c
1	C_{HEL}—C≡C	1.196(3)	1.197(2)	1.196(3)	1.201(3)
2	C_{HEL}—C≡C	1.437(3)	1.424(2)	1.430(3)	1.429(2)
3	angle α	177.6(3)	176.3(2)	172.0(2)	169.5(2)
4	helical pitch	2.709(2)	2.696(2)	2.725(2)	–
5	dihedral angle	50.7(2)	49.4(1)	49.1(2)	–

[a] For compounds **4**, the helical pitch (Å) is the distance between the two overlapping oxygen atoms of the helicene and the helical angle (°) is defined by the dihedral angle between carbons *a-b-c-d*.

(Table 1, entry 3). For **4c, 4d** and **4f**, the helicene core deformation was characterized by measuring both helical dihedral angles and helical pitch values (entries 4 and 5) which were not only similar among compounds **4c, 4d** and **4f** but also with previously reported derivatives.[4a,5k,6a,7a,10]

Finally, and of importance to explain some of the NMR behavior that will be later detailed, it is necessary to remember that substituents at position 6 of the helicene induce a strong conformational constraint onto the neighboring N-alkyl chains.[7a] In previously reported crystal structures and studies, it has been observed that added functional groups have an impact on the neighboring n-propyl chains and, in consequence, these residues adopt *gauche* conformations that fold above the helical core (Figure 2).[7a,11] This is here the case for compounds **4c, 4d** and **4f** in the solid state (Table 1, structures **A**–**C**). Then, as a result in ¹H NMR spectroscopy, the terminal methyl groups are shifted at lower frequency by −0.6 to −0.8 ppm. The ¹H NMR spectra of these three derivatives display similar low-frequency $\Delta\delta$ shifts of ca. −0.64 ppm for the methyl group of the constrained propyl chains. It is a general observation for the other derivatives **4** (see Supporting Information). For DAOTA **5c**, it was then interesting to observe, in the crystal structure, classical *anti* conformations for all propyl groups, and those next to the alkynyl substituent in particular. Since, for **5c** and all other DAOTA derivatives, only a weak $\Delta\delta$ shift of ca. −0.1 ppm occurs in ¹H NMR spectra (Figure 2), it is then likely that the two n-propyl chains present similar geometries in solution and hence a preferred *anti-anti* conformation as observed in the solid state. The relevance of this observation and a DFT confirmation will be later discussed.

In terms of electrochemistry, the redox behavior of cationic **4** and **5** is strongly dominated by their triarylcarbenium nature and their naturally high cation stability (Figure 3).[2l,7] In the range studied by cyclic voltammetry, DMQAs **4** exhibit three redox states accessible by mono-electronic oxidations and reductions (Figures S67–S74).[12] In anhydrous acetonitrile with tetrabutylammonium hexafluorophosphate as supporting electrolyte, cationic **4b** to **4h** can be *pseudo* reversibly oxidized to the corresponding radical dication **4**•++, from +0.78 to +0.97 V *vs.* ferrocene/ferrocenium (Fc/Fc+).
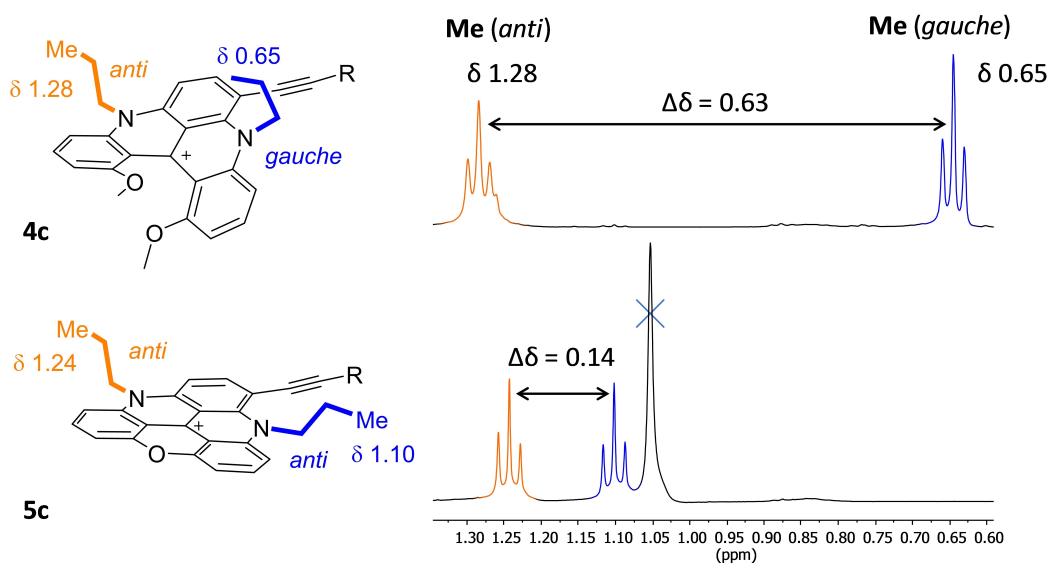
Figure 2. Left: Predominant geometries for acetylene derivatives **4** and **5** with corresponding *anti-gauche* and *anti-anti* conformations for the propyl side chains. Right: Chemical shift differences ($\Delta\delta$) in ¹H NMR spectroscopy between the two terminal methyl groups.
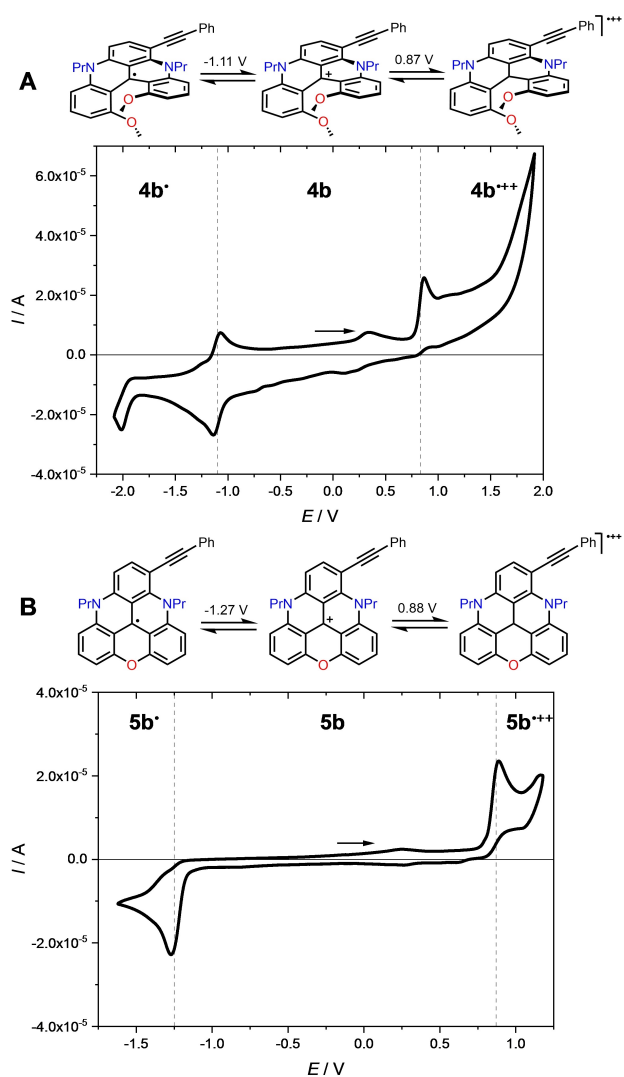
Chemistry–A European Journal

Research Article
doi.org/10.1002/chem.202104405

Chemistry Europe
European Chemical
Societies Publishing

Figure 3. Cyclic voltammograms of compounds A) **4b** and B) **5b** in acetonitrile ([TBA][PF$_6$] 0.1 M) at a Pt electrode, potential (V), versus Fc/Fc+.

Reversible mono-electronic reduction to the neutral radical **4**• happens at potentials from −1.09 to −1.24 V vs. Fc/Fc+. This reactivity is highlighted for **4b** in Figure 3 (part **A**) and noticeable differences can be seen for analogous **5b** (Figure 3, part **B**). In fact, for DAOTA **5a** to **5h**, while the overall pattern is similar with shifted values for the oxidation and reduction of the carbenium ion, from +0.82 to +1.02 V and −1.15 to −1.30 V vs. Fc/Fc+ respectively, pseudo-reversible reductions are this time observed. While reductions to radicals **4**• and **5**• are essentially unperturbed by the nature of the alkynyl side chains, a moderate influence can be observed in the oxidation of **4** and **5** to species **4**•++ and **5**•++ respectively. In fact, substrates carrying electron-rich and electron-poor aryl substituents on the triple bond present slightly easier and harder oxidations respectively.[13] Globally, the overall electronic impact of the substituents is rather modest and augured similar absorption properties for the organic dyes.

In fact, in absorption spectroscopy, the addition of terminal alkynyl substituents on the quinacridinium and triangulenium skeletons had only little impact (Figure 4, **A** and **C**). For instance, for compound **4a**, the first absorption band shifted from 5 nm only (621 vs. 616 nm for **4a** and **1**) and the trend was found to be the same with molar extinction coefficients (13400 M$^{−1}$cm$^{−1}$ for **4a** vs. 14000 M$^{−1}$cm$^{−1}$ for **1**).[7a] This behavior is reproduced for DAOTA **5a** with a slightly bigger red-shift in absorbance (569 vs. 557 nm for **5a** and **2**), and similar molar extinction coefficients.[5d] However, in emission spectroscopy (Figure 4, **B** and **D**), differences were more noticeable. For example, **4a** showed a bathochromism of 26 nm with photoluminescence quantum yield (PLQY) of 0.08, similar to that of **1**.[7a] For **5a**, a red-shifted emission by 22 nm and an increase of PLQY reaching 0.51 are observed.[7b]

Then, for the substituted derivatives, the influence of the different aryl groups was studied (Figure 4). First, DMQA **4b** (Ar = Ph) presented the lowest-energy band centered at 634 nm with a molar extinction of 9700 M$^{−1}$cm$^{−1}$ (Table 2, entry 3). The emission of **4b** is characterized by a maximum at 728 nm and a PLQY of 0.01; compound **4b** exhibits thus the most red-shifted emission spectrum, albeit weak, recorded for DMQA derivatives.[7a] In case of electron-rich aryl substituents, for example **4e** or **4h**, absorption spectra were very similar and emission properties could not be detected in solution. With electron-poor aryl derivatives **4c**, **4d**, **4f** and **4g**, the situation was quite different with an expected blue shift measured in both absorbance and fluorescence.[7a] In addition, the electron withdrawing groups slightly increased the PLQY, up to 0.05.

In the triangulenium series, a stronger contrast was noticed among the various derivatives **5b** to **5h**. In fact, while most compounds **5** presented very similar lowest-energy absorption bands (Table 2, entries 12 to 18), electron-rich derivative **5e** (Ar = 4-MeOPh) demonstrated a strong weakening of the molar absorption coefficient (8600 M$^{−1}$cm$^{−1}$ only, entry 15). Yet, the most interesting results came from emission spectroscopy. In this series, all compounds **5** were luminescent and, as expected, electron-rich **5e** and **5h** displayed red-shifted emissions, up to 23 nm compared to **5b**, whereas electron-poor compounds **5c**, **5d**, **5f** and **5g** showed a hypsochromic behavior, down by 18 nm. Furthermore, PLQYs show a clear and expected trend of stronger values for electron-poor compounds, up to 0.28 for **5f** that drop to 0.02 for electron-rich **5e** and **5h**.

Finally, as previously mentioned, when NMR spectroscopic analyses were performed to characterize DAOTA compounds **5**, ^{1}H NMR spectra displayed major differences in comparison to DMQA analogues **4** (Figure 5). In fact, for derivatives **5**, methylene protons α to the nitrogen atoms presented two very different situations: on one hand, a classical triplet-like signal assigned to the NC**H**$_2$ protons of the unhindered propyl chain (δ_{avg} 4.51 ppm, orange signal); on the other hand, a very broad signal around the 5.0 ppm region which corresponds to the NC**H**$_2$ hydrogen atoms adjacent to the alkynyl side chains (blue signal). This observation is general for all DAOTA derivatives **5** and is displayed for **5a** in Figure 5 (top). In contrast, spectra of derivatives **4** are typical of chiral derivatives, with well-distinguished diastereotopic NC**H**$_2$ protons (**4a**, Figure 5 bot-
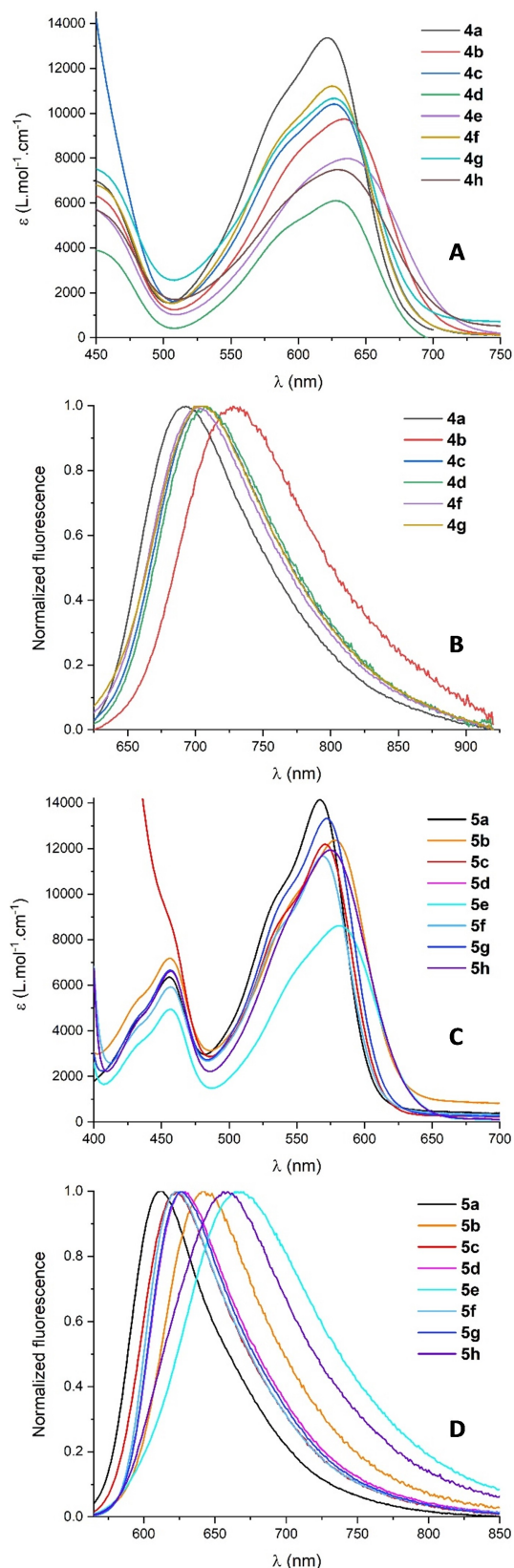
Chemistry–A European Journal

Research Article
doi.org/10.1002/chem.202104405

Chemistry Europe
European Chemical
Societies Publishing

Figure 4. Compounds **4**: A) Absorption and B) emission ($\lambda_{exc} = 610$ nm) spectra in acetonitrile. Compounds **5**: C) Absorption and D) emission ($\lambda_{exc} = 540$ nm) spectra in acetonitrile.

tom). The disparity between the spectra was striking, and particularly the presence of the broad band for compounds **5** (blue signal) positioned quite exactly between the analogous diastereotopic protons of derivatives **4**. This was indicative of a potential stereodynamic process for the DAOTA moieties, despite the achiral nature of the triangulenium core.

To investigate this possibility, variable temperature (VT) NMR experiments were performed on DAOTA salts [**5a**][BF$_4$] and [**5f**][BF$_4$]. The salts were dissolved in chloroform-*d* or in CD$_3$CN, and the solutions were analyzed by ^{1}H NMR spectroscopy at low or elevated temperatures respectively ($-55\,°C \leq T \leq 70\,°C$).[14] As suspected, the broad signal observable at 298 K was influenced by the change of temperature. It disappeared essentially at 268 K, only to reappear at 248 K and lower temperatures in the form of two well separated signals integrating for one proton each, for example at 5.78 and 4.14 ppm respectively, for salt [**5f**][BF$_4$] (Figure 6, short blue arrows). As evidenced, a dynamic conformational isomerism occurs which will be later defined and characterized (see below). For the measurement of the activation barriers ($\Delta G^{\ddagger}$), a line-shape analysis could not be pursued in view of the undefined nature of the broadened exchange signals. Assuming a singlet nature for these signals, the relationship $\Delta G^{\ddagger} = RT_c$ ($22.96 + \ln(T_c/\Delta\nu)$) was used with T_c being the coalescence temperature and $\Delta\nu$ the frequency separation of the peaks at low temperature. For salts [**5a**][BF$_4$] and [**5f**][BF$_4$], the resulting activation energies $\Delta G^{\ddagger}$ are equal to 11.8 and 12.6 kcal mol^{-1} respectively.[15]

With these results in hand, care was taken to (i) investigate the origin of the stereodynamic exchange of the N–CH$_2$ protons positioned next to the triple bond (Figure 6, blue signal) and (ii) determine the reasons for their very large chemical shift difference at low temperature, for example $\Delta\delta$ 1.64 ppm for **5f** at 218 K. This was not evident initially since DAOTA derivatives **5**, unlike their helicene counterparts, are composed of achiral cationic triangulene cores made of six aromatic rings that are coplanar to each other. This lack of asymmetry of the triangulene moiety has been well established in previous studies, that of Laursen and collaborators in particular.[2j] With that in mind, to explain the stereodynamic exchange, chiral conformations involving the nitrogen side chains and their relationship to the adjacent alkynyl substituents were looked for.

In retrospect, we realized that conformations displayed in Figures 6 and 7 for compounds **5**, based on solid state (X-ray) and solution (NMR) analyses, are presenting a typical case of planar chirality. In fact, for each compound **5**, there are two possible orientations for the (blue) propyl chains that bring about enantiomeric planar chiral conformations. In Figure 7, the drawings are represented in slightly different orientations to focus on the N–CH$_2$CH$_2$CH$_3$ chains and the subsequent stereogenic nitrogen atoms. Two opposite configurations are described, including the priority among the substituents that surround the N-atoms and the corresponding S_p and R_p descriptors.

To extend the stereodynamic analysis, an ion pairing of cations **5** with hexacoordinated phosphorus TRISPHAT **8** was

Chem. Eur. J. **2022**, *28*, e202104405 (6 of 11)

© 2022 The Authors. Chemistry - A European Journal published by Wiley-VCH GmbH

Chemistry–A European Journal

Research Article
doi.org/10.1002/chem.202104405

Chemistry
Europe
European Chemical
Societies Publishing

Table 2. Redox and optical properties of DMQA- FG derivatives **1**, **4a–4h** and DAOTA-FG derivatives **2**, **5a–5h**.

Entry	Compound	FG[a]	$E_{1/2}^{red\ [b]}$	$E_{1/2}^{ox\ [b]}$	$\lambda_{abs}^{[c]}$	$\varepsilon^{[d]}$	$\lambda_{em}^{[c]}$	Stokes shift[e]	Quantum yield[f]
1	1	H	−1.23	0.88	616	14000	667	1241	0.13
2	4a	CC-H	−1.24	0.96	621	13400	693	1673	0.08
3	4b	CC-Ph	−1.11	0.87	634	9700	728	2037	0.01
4	4c	CC-4-NO₂Ph	−1.09	0.97	627	10400	707	1805	0.04
5	4d	CC-4-CNPh	−1.09	0.96	628	6100	707	1779	0.03
6	4e	CC-4-OMePh	−1.12	0.78	636	8000	–	–	< 0.01
7	4f	CC-3,5-(CF₃)₂Ph	−1.09	0.92	625	11200	701	1735	0.05
8	4g	CC-2-pyridine	−1.09	0.92	627	10700	704	1744	0.04
9	4h	CC-2-thiophene	−1.10	0.84	629	7500	–	–	< 0.01
10	2	H	−1.36	0.99	557	14000	591	1030	0.42
11	5a	CC-H	−1.30	0.99	569	14100	613	1261	0.51
12	5b	CC-Ph	−1.15	1.02	579	12400	641	1671	0.14
13	5c	CC-4-NO₂Ph	−1.27	1.00	571	12200	623	1462	0.25
14	5d	CC-4-CNPh	−1.25	0.99	572	12700	629	1584	0.17
15	5e	CC-4-OMePh	−1.28	0.82	582	8600	664	2122	0.02
16	5f	CC-3,5-(CF₃)₂Ph	−1.27	0.97	569	11700	623	1523	0.28
17	5g	CC-2-pyridine	−1.24	0.96	572	13300	626	1508	0.25
18	5h	CC-2-thiophene	−1.22	0.87	575	11900	656	2147	0.02

[a] Functional group [b] Oxidation and reduction potential values measured by Cyclic Voltammetry for 10^{-3} M solution of DMQA derivatives **4a–4h** and **5a–5h** in acetonitrile ([TBA][PF₆]; 0.1 M) at a Pt electrode, Potential (V), versus the ferrocene/ferrocenium redox couple (Fc/Fc +). [c] in nm, recorded in acetonitrile solutions (10^{-5} M). [d] in $M^{-1}cm^{-1}$. [e] in cm^{-1}. [f] relative to Cresyl Violet (QY = 0.56 in EtOH), with $\lambda_{exc} = 590$ nm (entries 2–9) and with $\lambda_{exc} = 540$ nm (entries 11–18).

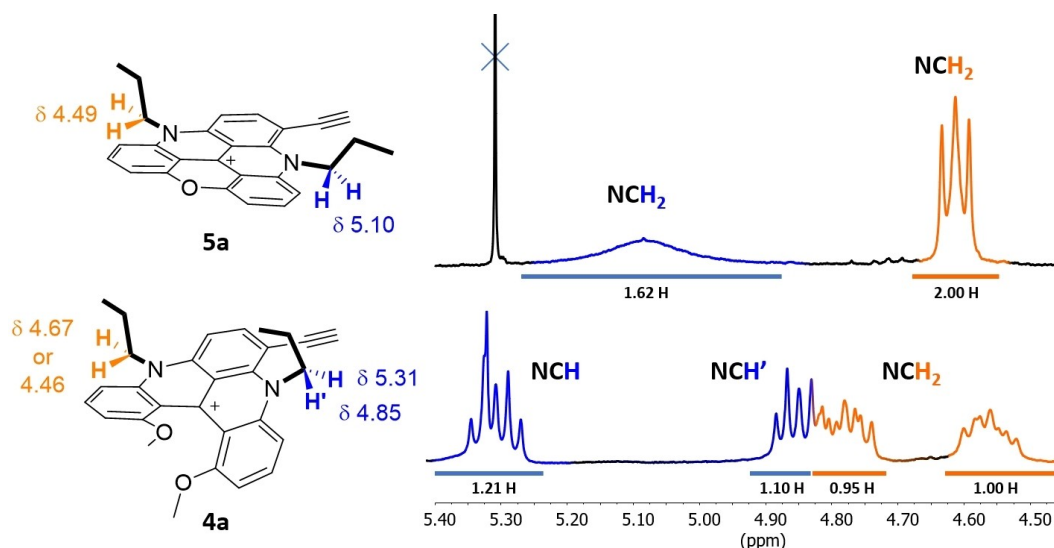**Figure 5.** Room-temperature ^{1}H NMR spectra of salts [**5a**][BF₄] and [**4a**][BF₄] (298 K, δ 5.4–4.45 ppm).

considered.[16] This chiral anion is known to be a general NMR chiral solvating, resolving and asymmetry-inducing reagent with chiral cationic species.[5a,17] When associated with configurationally labile cations, supramolecular diastereoselective interactions occur and one diastereomeric ion pair may become predominant in solution (*Pfeiffer* Effect).[17b,c] An association of configurationally labile **5** with anion **8** was thus considered for a discrimination and possibly a stereocontrol of the planar chiral geometry. Salt [**5f**][Δ-**8**] was prepared by ion pair metathesis, dissolved in chloroform-*d* and the chiral recognition (induction) studied by ^{1}H NMR spectroscopy from room to low temperatures (25 °C ≥ T ≥ −55 °C).

While the stereodynamic behavior of the constrained N–CH₂ (blue) protons remained essentially unchanged by the presence

of the chiral anion **8**, i.e., a broad signal at 298 K and a 1:1 split at 218 K ($\Delta\delta$ 1.63 ppm, Figure 8), the N–CH₂ protons of the sterically unhindered propyl chain displayed a marked influence of anion Δ-**8**. In effect, at room temperature, the (orange) triplet signal in Figure 6 (BF₄ salt) is transformed into two well-distinguished diastereotopic NCH₂ protons in Figure 8 (top, δ 4.60 and 4.43 ppm), a change induced by the NMR chiral solvating TRISPHAT anion.[17c] At low temperature (218 K), one of these two protons splits further in two sets of signals. One part is observable around δ 4.64 ppm while the other part overlaps with the other diastereotopic proton (δ ca. 4.38 ppm). This NMR enantiodifferentiation and its consequence on the integration of the signals is detailed in Figure S57.
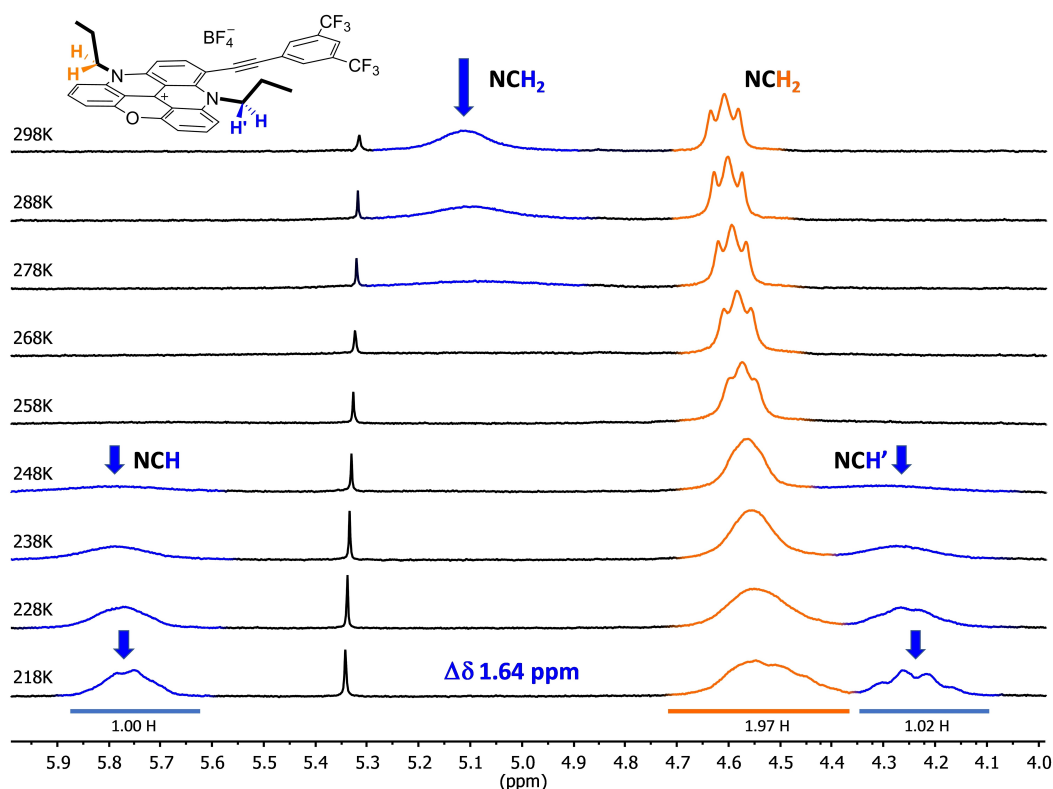
Chemistry–A European Journal

Research Article
doi.org/10.1002/chem.202104405

Chemistry
Europe
European Chemical
Societies Publishing

Figure 6. Salt [**5 f**][BF$_4$], ^{1}H VT NMR spectra (δ 6.0–4.0 ppm, 298 K to 218 K).
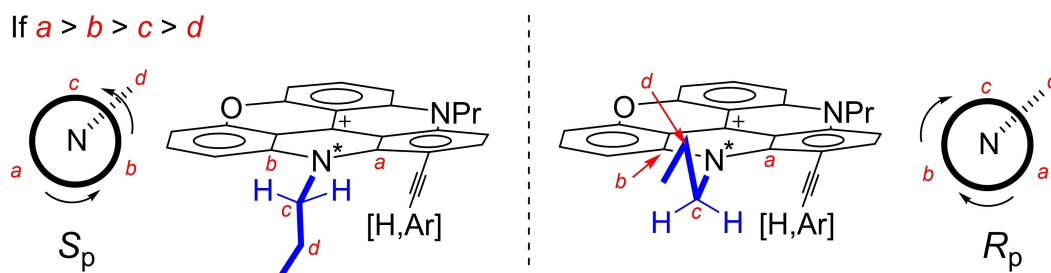

Figure 7. Planar chiral conformations for derivatives **5** and corresponding absolute S_p and R_p configurations, including priorities $a>b>c>d$ for substituents that surround the stereogenic N-atoms.

This leads to a quite unusual integration for the methylene protons next to the N-atoms (Figure 8, bottom): 1.00 (H blue), 0.69 (H orange), 1.33 (H orange) and 1.06 (H blue), from high to low frequencies. This phenomenon can only be explained thanks to the NMR differentiating and inducing ability of TRISPHAT onto the S_p and R_p conformations of cation **5 f** at low temperature.[18] In fact, the presence of anion Δ-**8** not only helps the NMR enantiodifferentiation of the two planar chiral conformations but, due to the chemical differences among diastereomeric [S_p-**5 f**][Δ-**8**] and [R_p-**5 f**][Δ-**8**] salts, the preferred formation of one of the two ion pairs occurs.[19] A moderate yet noticeable asymmetric induction (*Pfeiffer* effect) is achieved with a 0.68:0.32 diastereomeric ratio. VT-ECD experiments on CHCl$_3$ solutions of [**5 f**][Δ-**8**] were performed (298–213 K, Figure S66) and did not reveal any chiroptical induction in the UV/

vis spectrum of the corresponding salt; this result being actually expected knowing that the induction corresponds only to a stereocontrol of the aliphatic side chain with little interaction with the planar chromophore.

Finally, with these experimental evidences in hand, DFT calculations were pursued to clarify even further the stereochemical phenomenon. First, the conformational population of complex **5 a** was investigated in silico. Of importance, of the two conformations already considered, the *anti-anti* geometry (S_p and R_p conformations) is preferred (more stable) over the *anti-gauche* geometry by 1.1 kcal mol^{-1} (Figure 9, **A** and **B**). In addition, we could reproduce computationally the kinetic barrier obtained for the rotation of the propyl chain attached to the stereogenic nitrogen atom. Satisfactorily, with a calculated value of 10.7 kcal mol^{-1} in the free energy surface, a very good
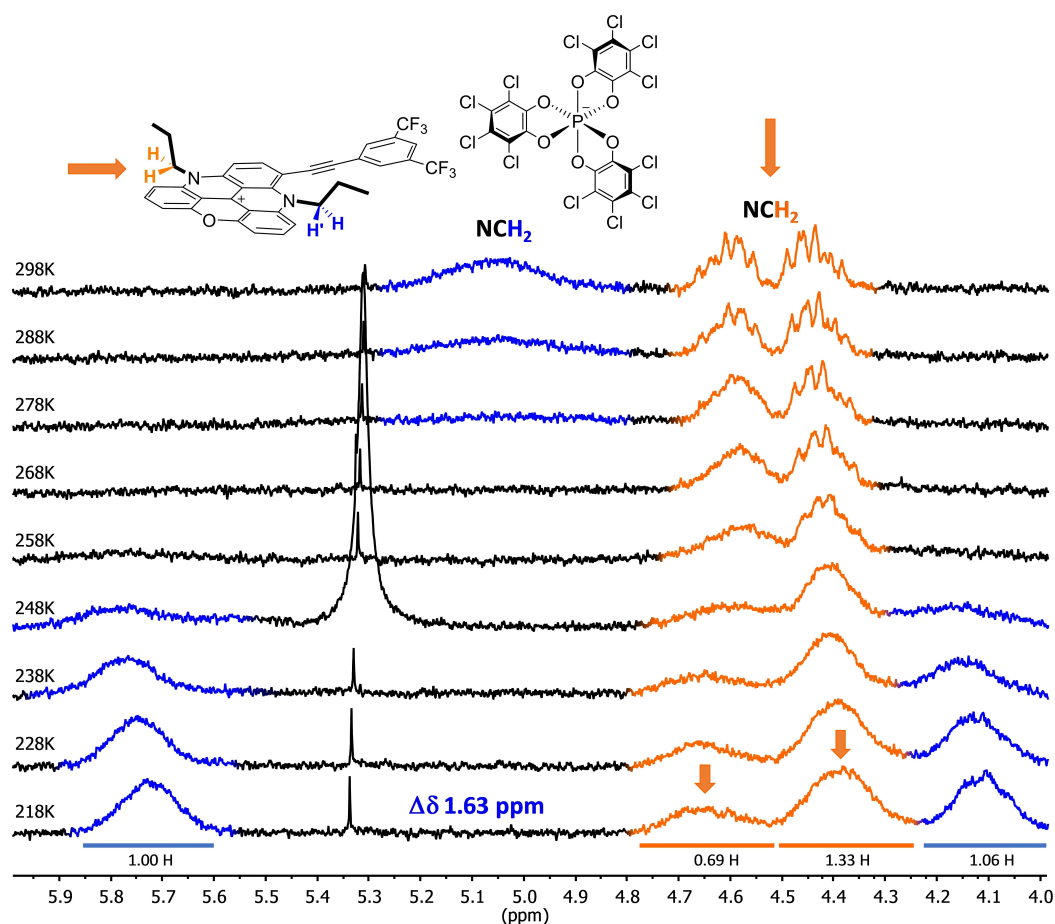
Chemistry–A European Journal

Research Article
doi.org/10.1002/chem.202104405

Chemistry Europe
European Chemical
Societies Publishing

Figure 8. Salt [**5f**][Δ-**TRISPHAT**], ^{1}H VT NMR spectra (δ 6.0–4.0 ppm, 298 K to 218 K). At 248 K, a parasite signal appears around 5.3 ppm which has no bearing on the overall experiment.

agreement with the experimental measurement is obtained ($\Delta G^{\pm}_{exp}$ 11.8 kcal mol^{-1} by VT NMR). Finally, encouraged by the close agreement between experimental and computational values, the NMR spectrum of compound **5a** was calculated (Figure 9, C and Figure S75). To our delight, the computed spectrum reproduces the strong differentiation occurring between the two constrained diastereotopic N–CH$_2$ protons. In fact, the very large difference in experimental chemical shifts ($\Delta\delta_{exp}$ 1.64 ppm) is well replicated by the obtained theoretical values of 5.97 and 4.06 ppm for the blue protons nearest and most distant from the acetylene fragment, respectively. These values could be further corrected to δ 5.66 and 3.86 by applying linear scaling factors found in the literature.[20]

Conclusion

In summary, series of acetylene derivatives of cationic diazaoxa triangulenes (DAOTA) and [4]helicenes (DMQA) were prepared. These C≡C-functionalized products are for the most fluorescent, with red-shifted absorptions ($\Delta\lambda_{abs}$ up to 25 nm) and emissions ($\Delta\lambda_{em}$ up to 73 nm, Φ_{PL} up to 51%). With for DAOTA-based derivatives **5**, a dynamic stereoisomerism phenomenon was

evidenced for the first time. At low temperature in ^{1}H NMR spectroscopy (218 K), N–CH$_2$ protons become diastereotopic with chemical shifts differences ($\Delta\delta$) as high as +1.64 ppm. The signal coalescence occurs around 273 K with a barrier of $\sim$12 kcal mol^{-1}. This phenomenon is due to planar chiral conformations (S_p and R_p configurations, Figure 7), induced by the geometry of the alkyl (propyl) side-chains next to the acetylenic substituents. Ion pairing studies with Δ-TRISPHAT anion not only confirmed the occurrence of the chiral conformations but evidenced an asymmetric induction from the chiral phosphorus(V) anion onto the cation (d.r. 68:32). DFT calculations further confirmed the preferred *anti-anti* geometries, stereodynamics and the peculiar behavior.

Supporting Information

Supporting Information for this article is given via a link at the end of the document. It contains experimental conditions, characterizations of all new compounds, UV-Vis and fluorescence spectra and computational details.

Deposition Number(s) 2123630, 2123631, 2123632, 2123633 contain(s) the supplementary crystallographic data for this
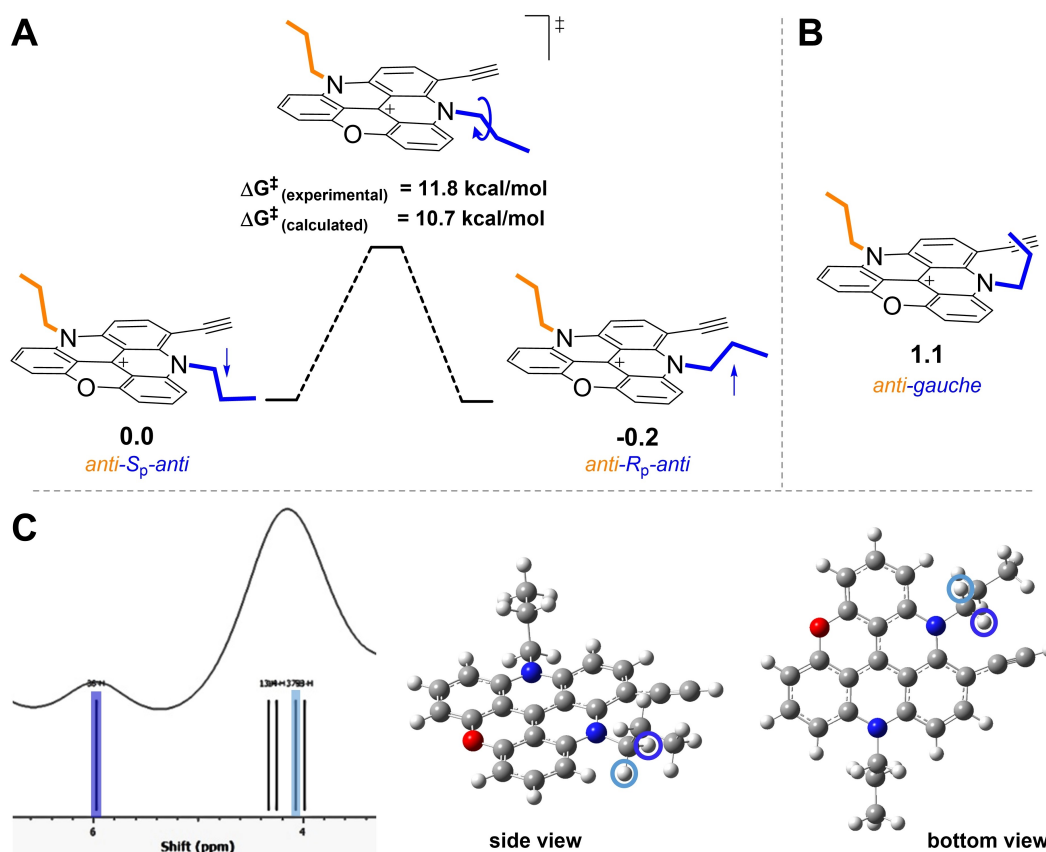
Chemistry–A European Journal

Research Article
doi.org/10.1002/chem.202104405

**Chemistry
Europe**
European Chemical
Societies Publishing

Figure 9. Conformational population and calculated ^{1}H NMR spectrum (δ 6.8–3.3 ppm) for derivative **5a**. Key diastereotopic N–CH$_2$ protons are highlighted (blue and light blue colors).

paper. These data are provided free of charge by the joint Cambridge Crystallographic Data Centre and Fachinformationszentrum Karlsruhe Access Structures service.

In addition, the dataset for this article can be found at the following DOI: 10.26037/yareta:7iyohmxz7fgcjjuked6ivbog6u. It will be preserved for 10 years.

Acknowledgements

Conflict of Interest

The authors declare no conflict of interest.

Data Availability Statement

The data that support the findings of this study are openly available in yareta.unige.ch at https://doi.org/10.26037/yareta:7iyohmxz7fgcjjuked6ivbog6u, reference number 4008.

[1] D. F. Duxbury, *Chem. Rev.* **1993**, *93*, 381–433.
[2] a) B. W. Laursen, F. C. Krebs, *Angew. Chem. Int. Ed.* **2000**, *39*, 3432–3434; *Angew. Chem.* **2000**, *112*, 3574–3576; b) B. W. Laursen, F. C. Krebs, *Chem. Eur. J.* **2001**, *7*, 1773–1783; c) Y. Shen, C.-F. Chen, *Chem. Rev.* **2011**, *112*, 1463–1535; d) M. Gingras, *Chem. Soc. Rev.* **2013**, *42*, 968–1006; e) M. Gingras, G. Felix, R. Peresutti, *Chem. Soc. Rev.* **2013**, *42*, 1007–1050; f) M. Gingras, *Chem. Soc. Rev.* **2013**, *42*, 1051–1095; g) J. Bosson, J. Gouin, J. Lacour, *Chem. Soc. Rev.* **2014**, *43*, 2824–2840; h) I. Bora, S. A. Bogh, M. Rosenberg, M. Santella, T. J. Soerensen, B. W. Laursen, *Org. Biomol. Chem.* **2016**, *14*, 1091–1101; i) C. Li, Y. Yang, Q. Miao, *Chem. Asian J.* **2018**, *13*, 884–894; j) M. Rosenberg, K. R. Rostgaard, Z. Liao, A. Ø. Madsen, K. L. Martinez, T. Vosch, B. W. Laursen, *Chem. Sci.* **2018**, *9*, 3122–3130; k) K. Dhbaibi, L. Favereau, J. Crassous, *Chem. Rev.* **2019**, *119*, 8846–8953; l) M. Rosenberg, M. Santella, S. A. Bogh, A. V. Muñoz, H. O. B. Andersen, O. Hammerich, I. Bora, K. Lincke, B. W. Laursen, *J. Org. Chem.* **2019**, *84*, 2556–2567.
[3] a) O. Kel, A. Fürstenberg, N. Mehanna, C. Nicolas, B. Laleu, M. Hammarson, B. Albinsson, J. Lacour, E. Vauthey, *Chem. Eur. J.* **2013**, *19*,

7173–7180; b) A. Babič, S. Pascal, R. Duwald, D. Moreau, J. Lacour, E. Allémann, *Adv. Funct. Mater.* **2017**, *27*, 1701839; c) C. Bauer, R. Duwald, G. M. Labrador, S. Pascal, P. Moneva Lorente, J. Bosson, J. Lacour, J.-D. Rochaix, *Org. Biomol. Chem.* **2018**, *16*, 919–923; d) B. W. Lewis, N. Bisballe, M. Santella, P. A. Summers, J.-B. Vannier, M. K. Kuimova, B. W. Laursen, R. Vilar, *Chem. Eur. J.* **2021**, *27*, 2523–2536; e) P. A. Summers, A. P. Thomas, T. Kench, J.-B. Vannier, M. K. Kuimova, R. Vilar, *Chem. Sci.* **2021**, *12*, 14624–14634.

[4] a) L. Mei, J. M. Veleta, J. Bloch, H. J. Goodman, D. Pierce-Navarro, A. Villalobos, T. L. Gianetti, *Dalton Trans.* **2020**, *49*, 16095–16105; b) L. Mei, J. M. Veleta, T. L. Gianetti, *J. Am. Chem. Soc.* **2020**, *142*, 12056–12061; c) L. Mei, T. Gianetti, *Synlett* **2021**, *32*, 337–334; d) L. Mei, J. Moutet, S. M. Stull, T. L. Gianetti, *J. Org. Chem.* **2021**, *86*, 10640–10653.

[5] a) C. Herse, D. Bas, F. C. Krebs, T. Bürgi, J. Weber, T. Wesolowski, B. W. Laursen, J. Lacour, *Angew. Chem. Int. Ed.* **2003**, *42*, 3162–3166; *Angew. Chem.* **2003**, *115*, 3270–3274; b) O. Kel, P. Sherin, N. Mehanna, B. Laleu, J. Lacour, E. Vauthey, *Photochem. Photobiol. Sci.* **2012**, *11*, 623–631; c) J. Elm, J. Lykkebo, T. J. Sørensen, B. W. Laursen, K. V. Mikkelsen, *J. Phys. Chem. A* **2012**, *116*, 8744–8752; d) C. Adam, A. Wallabregue, H. Li, J. Gouin, R. Vanel, S. Grass, J. Bosson, L. Bouffier, J. Lacour, N. Sojic, *Chem. Eur. J.* **2015**, *21*, 19243–19249; e) R. Duwald, S. Pascal, J. Bosson, S. Grass, C. Besnard, T. Bürgi, J. Lacour, *Chem. Eur. J.* **2017**, *23*, 13596–13601; f) H. Li, S. Voci, A. Wallabregue, C. Adam, G. M. Labrador, R. Duwald, I. Hernández Delgado, S. Pascal, J. Bosson, J. Lacour, L. Bouffier, N. Sojic, *ChemElectroChem* **2017**, *4*, 1750–1756; g) H. Li, A. Wallabregue, C. Adam, G. M. Labrador, J. Bosson, L. Bouffier, J. Lacour, N. Sojic, *J. Phys. Chem. C* **2017**, *121*, 785–792; h) S. A. Bogh, M. Simmermacher, M. Westberg, M. Bregnhøj, M. Rosenberg, L. De Vico, M. Veiga, B. W. Laursen, P. R. Ogilby, S. P. A. Sauer, T. J. Sørensen, *ACS Omega* **2017**, *2*, 193–203; i) Z. Jarolímová, J. Bosson, G. M. Labrador, J. Lacour, E. Bakker, *Electroanalysis* **2018**, *30*, 1378–1385; j) Z. Jarolímová, J. Bosson, G. M. Labrador, J. Lacour, E. Bakker, *Electroanalysis* **2018**, *30*, 650–657; k) R. Duwald, J. Bosson, S. Pascal, S. Grass, F. Zinna, C. Besnard, L. Di Bari, D. Jacquemin, J. Lacour, *Chem. Sci.* **2020**, *11*, 1165–1169; l) M. Marinova, S. Pascal, L. Guénée, C. Besnard, B. Shivachev, K. Kostova, C. Villani, R. Franzini, V. Dimitrov, J. Lacour, *J. Org. Chem.* **2020**, *85*, 11908–11923; m) C. R. Benson, L. Kacenauskaite, K. L. VanDenburgh, W. Zhao, B. Qiao, T. Sadhukhan, M. Pink, J. Chen, S. Borgi, C.-H. Chen, B. J. Davis, Y. C. Simon, K. Raghavachari, B. W. Laursen, A. H. Flood, *Chem* **2020**, *6*, 1978–1997; n) J. Bosson, G. M. Labrador, C. Besnard, D. Jacquemin, J. Lacour, *Angew. Chem. Int. Ed.* **2021**, *60*, 8733–8738; *Angew. Chem.* **2021**, *133*, 8815–8820; o) L. Kacenauskaite, N. Bisballe, R. Mucci, M. Santella, T. Pullerits, J. Chen, T. Vosch, B. W. Laursen, *J. Am. Chem. Soc.* **2021**, *143*, 1377–1385; p) J. Bosson, N. Bisballe, B. W. Laursen, J. Lacour, in *Helicenes. Synthesis, Properties and Applications* (Eds.: J. Crassous, I. G. Stara, I. Stary), Wiley-VCH, **2021**, p. in press.

[6] a) A. C. Shaikh, J. Moutet, J. M. Veleta, M. M. Hossain, J. Bloch, A. V. Astashkin, T. L. Gianetti, *Chem. Sci.* **2020**, *11*, 11060–11067; b) V. Kiran, S. P. Mathew, S. R. Cohen, I. Hernández Delgado, J. Lacour, R. Naaman, *Adv. Mater.* **2016**, *28*, 1957–1962.

[7] a) I. H. Delgado, S. Pascal, A. Wallabregue, R. Duwald, C. Besnard, L. Guénée, C. Nançoz, E. Vauthey, R. C. Tovar, J. L. Lunkley, G. Muller, J. Lacour, *Chem. Sci.* **2016**, *7*, 4685–4693; b) I. H. Delgado, S. Pascal, C. Besnard, S. Voci, L. Bouffier, N. Sojic, J. Lacour, *Chem. Eur. J.* **2018**, *24*, 10186–10195.

[8] To the exception of carboxylate groups for which weak red-shifted emission remains for the corresponding DMQA and DAOTA derivatives, all other EDGs leads to a lack of emissive properties. In fact, in this series of compounds, the quantum efficiency of fluorescence declines progressively with the concomitant increase in emission wavelength, illustrating the effect of the energy gap law. See Ref. [7a] and [7b] for details and further explanations.

[9] C. Wu, F. Ye, G. Wu, G. Xu, G. Deng, Y. Zhang, J. Wang, *Synthesis* **2016**, *48*, 751–760.

[10] P. Moneva Lorente, A. Wallabregue, F. Zinna, C. Besnard, L. Di Bari, J. Lacour, *Org. Biomol. Chem.* **2020**, *18*, 7677–7684.

[11] For **4c** specifically, half of the unit cell contains a molecule of **4c** with an *anti* conformation for the n-propyl chain. This is probably due to packing interactions that modify the gauche preference.

[12] T. J. Sørensen, M. F. Nielsen, B. W. Laursen, *ChemPlusChem* **2014**, *79*, 1030–1035.

[13] The presence of strong EWG induces extra redox chemistry, in reduction in particular. See Figures S68, S69, S72.

[14] For salt [**5a**][BF$_4$], NMR experiments were performed in CD$_2$Cl$_2$ and CD$_3$CN for low and high temperature VT experiments respectively. Very similar results to [**5f**][BF$_4$] are obtained.

[15] For salts [**5a**][BF$_4$] and [**5f**][BF$_4$], measurements were performed on 500 and 300 MHz instruments. The following T_c and $\Delta\nu$ values were found. For **5a**: 273 K and 852 Hz. For **5f**: 283 K and 465 Hz.

[16] J. Lacour, C. Ginglinger, C. Grivet, G. Bernardinelli, *Angew. Chem. Int. Ed. Engl.* **1997**, *36*, 608–609; *Angew. Chem.* **1997**, *109*, 660–662.

[17] a) J. Lacour, S. Barchéchath, J. J. Jodry, C. Ginglinger, *Tetrahedron Lett.* **1998**, *39*, 567–570; b) J. J. Jodry, R. Frantz, J. Lacour, *Inorg. Chem.* **2004**, *43*, 3329–3331; c) J. Lacour, D. Moraleda, *Chem. Commun.* **2009**, *46*, 7073–7089.

[18] a) H. Ratni, J. J. Jodry, J. Lacour, E. P. Kündig, *Organometallics* **2000**, *19*, 3997–3999; b) J. Giner Planas, D. Prim, F. Rose-Munch, E. Rose, D. Monchaud, J. Lacour, *Organometallics* **2001**, *20*, 4107–4110; c) J.-P. Djukic, A. Berger, M. Pfeffer, A. de Cian, N. Kyritsakas-Gruber, J. Vachon, J. Lacour, *Organometallics* **2004**, *23*, 5757–5767.

[19] a) H. S. Chow, E. C. Constable, R. Frantz, C. E. Housecroft, J. Lacour, M. Neuburger, D. Rappoport, S. Schaffner, *New J. Chem.* **2009**, *33*, 376–385; b) C. Pasquini, V. Desvergnes-Breuil, J. J. Jodry, A. Dalla Cort, J. Lacour, *Tetrahedron Lett.* **2002**, *43*, 423–426.

[20] G. K. Pierens, *J. Comput. Chem.* **2014**, *35*, 1388–1394.